# Optimising broadband pulses for DEER depends on concentration and distance range of interest

Andreas Scherer, Sonja Tischlik, Sabrina Weickert, Valentin Wittmann, Malte Drescher

Department of Chemistry and Konstanz Research School Chemical Biology, University of Konstanz, Konstanz, Germany

5    *Correspondence to:* Malte Drescher (malte.drescher@uni–konstanz.de)

**Abstract.** EPR distance determination in the nanometre region has become an important tool for studying the structure and interaction of macromolecules. Arbitrary waveform generators (AWGs), which have recently become commercially available for EPR spectrometers, have the potential to increase the sensitivity of the most common technique double electron-electron resonance (DEER, also called PELDOR), as they allow the generation of broadband pulses. There are several families of

10    broadband pulses, which are different in general pulse shape and the parameters that define them. Here, we compare the most common broadband pulses. When broadband pulses lead to a larger modulation depth they also increase the background decay of the DEER trace. Depending on the dipolar evolution time this can significantly increase the noise level towards the end of the form factor and limit the potential increase of the modulation to noise ratio (MNR). We found asymmetric hyperbolic secant (HS{1,6}) pulses to perform best for short DEER traces leading to a MNR improvement of up to 86 % compared to

15    rectangular pulses. For longer traces we found symmetric hyperbolic secant (HS{1,1}) pulses to perform best, however, the increase compared to rectangular pulses goes down to 43 %.

## 1 Introduction

In the last years DEER (double electron-electron resonance) has developed into an important technique for the determination of distances in the nanometre range (Jeschke, 2012, p.2; Milov et al., 1984; Salkhon, K.M. Milov, A.D., Shchirov, M.D., 1981)

20    and in particular into a suitable tool for studying biological macromolecules (e.g. proteins (Jeschke, 2012; Robotta Marta et al., 2014) or RNA/DNA (Grytz et al., 2017; Kuzhelev et al., 2018)). As many bio-macromolecules do not contain paramagnetic centres, for many DEER experiments spin labels are introduced with the help of site-directed spin labelling (Hubbell et al., 1998). Although many different types of spin labels have been introduced in the last years ranging from trityl (Abdullin et al., 2015; Jassoy et al., 2018), Gd(III) (Collauto et al., 2016; Dalaloyan et al., 2015; Mahawaththa et al., 2018), Copper(II) (Wort

25    et al., 2019) to photoexcitable spin labels (Di Valentin et al., 2014; Hintze et al., 2016), just to mention a few examples, nitroxide labels are still amongst the most widely used tags.

Increasing the sensitivity of DEER spectroscopy is an active field of research (Borbat et al., 2013; Breitgoff et al., 2017; Doll et al., 2015; Jeschke et al., 2004; Lovett et al., 2012; Milikisiyants et al., 2019; Polyhach et al., 2012; Tait and Stoll, 2016; Teucher and Bordignon, 2018). A very elegant approach to increasing DEER sensitivity has been made possible by the

30    availability of arbitrary waveform generators with time resolution in the nanosecond region as they allow the generation of broadband microwave pulses (Doll et al., 2013; Doll and Jeschke, 2017; Spindler et al., 2017).

Here, we compare nitroxide-nitroxide DEER performance for different types of broadband shaped pulses and identify the best parameters for each pulse type as well as the best pulse for different measurement and sample conditions. We show that the performance of the broadband pulses can depend on the required length of the DEER trace as well as the spin concentration.

35    A calculation shows what performance of shaped pulses can be expected for different trace lengths and spin concentrations.

The manuscript is organized as follows: In Sect. 1 we will give a brief overview over the pulse shapes that are compared in this manuscript. In Sect. 2, we will describe the experimental details and the compounds that have been used in this study. In Sect. 3, we will present and discuss the experimental results. We will first compare rectangular and Gaussian pulses for DEER spectroscopy and show that Gaussian pulses can yield a higher sensitivity than rectangular pulses. We will then compare

5    broadband pulses with rectangular and Gaussian pulses. After an optimisation of the parameters for broadband pulses, we will show that HS{1,1} and HS{1,6} have the highest sensitivity for nitroxide-nitroxide DEER. Finally, it will be shown that the performance of the pulses is dependent on the spin concentration as well as on the measured distance.

In magnetic resonance experiments, a pulse is generated by a time-dependent field $B_1$ that is applied perpendicular to the $B_0$ field which defines the z-direction. All pulses in this paper can be described in terms of an amplitude function $A(t)$ and a

10   frequency function $\omega(t)$.

The resulting $B_1$ field in the rotating frame is:

$$B_{1,x}(t) = A(t)\cos(\rho(t)),$$   (1)

$$B_{1,y}(t) = A(t)\sin(\rho(t)).$$   (2)

Where the phase $\rho(t)$ is defined as $\rho(t) = \int_0^t \omega(t')dt'$. Rectangular pulses are described by $\omega(t) = 0$ and $A(t) = B_1$ during

15   the pulse, i.e. by a $B_1$ field with a constant phase and intensity. The sidebands of the sinc-shaped excitation profile of rectangular pulses increase the overlap of the observer and pump pulse in DEER, resulting in so called '2+1' artefacts at the end of the DEER trace. It has recently been shown that those artefacts can be reduced by replacing the rectangular pulses with Gaussian pulses (Teucher and Bordignon, 2018). Gaussian pulses also have a frequency function of $\omega(t) = 0$ but an amplitude function:

20   $$A(t) = \exp\left(-\frac{4\ln(2)t^2}{FWHM^2}\right),$$   (3)

FWHM describes the full width at half maximum of the pulse in the time domain (Teucher and Bordignon, 2018). During a rectangular or Gaussian pulse the magnetisation vector is rotated around the $B_1$ field with an angle that is independent of the initial orientation of the magnetisation vector. Such pulses are therefore called uniform rotation pulses (Kobzar et al., 2012). As rectangular and Gaussian pulses have a fixed frequency, they are also referred to as monochromatic pulses.

25   One of the most significant challenges in EPR spectroscopy is the limited excitation bandwidth of rectangular and also Gaussian pulses compared to the width of many EPR spectra. In the case of nitroxide-nitroxide DEER, a significant part of the EPR spectrum does neither contribute to observing nor to pumping when using rectangular pulses.

Using broadband shaped pulses, the excitation bandwidth can be increased (Doll et al., 2013). Broadband shaped pulses distinguish from  rectangular and Gaussian pulses mainly in that they do not have a constant frequency, but the frequency is

30   swept over a given range during the pulse, which allows increasing the excitation bandwidth. In an accelerated frame, which rotates with the instantaneous excitation frequency of the pulse, the effective field rotates from the +z to the –z direction (Baum et al., 1985; Deschamps et al., 2008; Garwood and DelaBarre, 2001; Kupce and Freeman, 1996). Under adiabatic conditions the magnetisation follows the effective field on its way from +z to –z (Baum et al., 1985; Doll et al., 2013a). Pulses that induce this kind of spin flip behaviour are called point-to-point rotation pulses. This approach allows the generation of pulses that

35   have a large excitation bandwidth and that are, above a certain threshold, more insensitive to the resonator profile than rectangular pulses (Baum et al., 1985). Their ability to flip spins from the +z to the –z-axis makes such broadband shaped pulses perfect candidates for the pump pulse in the DEER pulse sequence. Their larger excitation profile has the potential to result in a larger modulation depth and therefore a larger sensitivity (Bahrenberg et al., 2017; Doll et al., 2015; Spindler Philipp E. et al., 2013; Tait and Stoll, 2016).

Intuitively, a high adiabaticity means that the effective magnetic field moves more slowly from +z to –z, making it easier for the spins to follow, thus resulting in a higher inversion efficiency.

The adiabaticity $Q$ is formally defined as (Kupce and Freeman, 1996):

$$Q = \frac{2\,\pi\nu_1}{|\mathrm{d}\theta/\mathrm{d}t|}. \tag{4}$$

5   Here, $\nu_1$ is the strength of the effective magnetic field and $\theta$ is its polar angle in the accelerated frame. The pulses have a good inversion efficiency, if $Q \gg 1$ (Deschamps et al., 2008). In general, the adiabaticity changes during the duration of the pulse and is different for spins with different frequency offsets. Adiabatic pulses are typically quantified by their minimum adiabaticity $Q_{\min}$.

Chirp pulses have a constant amplitude function and a linear frequency function $\omega(t) = f_{\text{start}} + pt$, where $p = \frac{\Delta f}{t_p}$ is a sweep

10  constant, $t_p$ is the pulse length and $\Delta f = f_{\text{end}} - f_{\text{start}}$. $f_{\text{start}}$ and $f_{\text{end}}$ are the start and end frequencies of the frequency sweep. The minimum adiabaticity $Q_{\min}$ is reached when a spin is on resonance with the pulse frequency (Doll et al., 2013a):

$$Q_{\min} = \frac{2\pi\nu_1^2 t_p}{\Delta f}, \tag{5}$$

$Q_{\min}$ increases with the pulse length but decreases with the sweep width. The frequency width for a pump pulse should be chosen such that a large part of the spectrum is excited without having significant spectral overlap with the pulses at the

15  observer frequency. The steep flanks at the beginning and the end of the rectangular amplitude profile lead to distortions in the excitation profiles of chirp pulses. Smoothing both ends of the pulses with a quarter sine-wave can reduce theses distortions (Bohlen and Bodenhausen, 1993). The smoothing can be adapted by changing the rising time $t_{\text{rise}}$. Following the logic so far, the pulse length should be chosen as long as possible to enable a very high adiabaticity. However, a broadband shaped pulse flips spins with different offsets at different times. When used as a pump pulse in DEER, this results in a shift of the dipolar

20  oscillations and an artificial broadening of smaller distances in the distance distribution. Therefore, the pulse length should be chosen such that (Breitgoff et al., 2019):

$$t_p < \frac{T_{dd}}{4}, \tag{6}$$

with the dipolar evolution time $T_{dd}$ of the shortest expected distance.

In addition to chirp pulses there are more elaborate pulses employing more elaborate frequency and amplitude functions. The

25  most common ones are WURST (wideband, uniform, smooth truncation) and HS (hyperbolic secant) pulses. The trends discussed so far are valid for them as well. However, they feature additional parameters that can be used to tune the steepness of the corresponding excitation profiles.

WURST pulses have a linear frequency sweep as well but a different amplitude function than chirp pulses (Kupce and Freeman, 1995b; Spindler et al., 2017):

30  $$A(t) = A_{\max}\left(1 - \left|\sin\left(\frac{\pi t}{t_p}\right)\right|^n\right), \tag{7}$$

The effect of the parameter $n$ determining the steepness of the amplitude function will be discussed below.

HS pulses have non-linear frequency sweeps and are described by the following amplitude and frequency functions:

$$A(t) = \operatorname{sech}\left(\beta 2^{h-1}\left(\frac{t}{t_p}\right)^h\right), \tag{8}$$

$$\omega(t) = \frac{\Delta f}{2} \tanh\left(\frac{\beta}{2}\right)^{-1} \tanh\left(\frac{\beta t}{t_p}\right),$$ (9)

with order parameter $h$ and truncation parameter $\beta$. The effects of $\beta$ will be discussed below. A common choice for $h$ is to set $h = 1$. These pulses have an offset-independent adiabaticity and a rather rectangular excitation profile (Baum et al., 1985; Tannús and Garwood, 1996). Increasing the order $h$ of an HS pulse will lead to a higher adiabaticity at the maximum of the

5    excitation profile but less steeper flanks (Breitgoff et al., 2019). A compromise can be found by using an asymmetric HS pulse where the flank close to the observer is made steep by an order of 1 and where the other flank has a higher order for a higher adiabaticity (Doll et al., 2016). Symmetric pulses with an order parameter of $h = 1$ will be referred to as HS{1,1}, asymmetric pulses where the first part of the pulse has on order parameter of $h = 1$ and the second half has $h = 6$, as suggested by Doll et al. (2016) are referred to as HS{1,6} (Doll et al., 2016).

10    The measured DEER-trace $V(t)$ is the product of the form factor $F(t)$ that contains the required intramolecular distance information and a background-function $B(t)$ (Jeschke, 2012):

$$V(t) = F(t) \cdot B(t),$$ (10)

The background decay is caused by the intermolecular interactions of the observer spin with pump spins of surrounding molecules. Assuming that the spins are homogenously distributed the background decay can be described by an exponential

15    decay:

$$B(t) = \exp(-kt^{d/3}),$$ (11)

where d is a dimensionality constant and the decay constant $k$ is described by the following equation (Pannier et al., 2000):

$$k = \frac{N_a \pi \mu_0}{9\sqrt{3}\hbar} g^2 \mu_e^2 f c,$$ (12)

Here, $c$ is the spin concentration, $f$ the inversion efficiency of the pump pulse, $\mu_e$ the Bohr-magneton, $\mu_0$ the magnetic field

20    constant, $N_a$ the Avogadro number and $g$ the isotropic g-factor of the nitroxide.

## 2 Materials and Methods

### 2.1 Sample preparation

Wheat germ agglutinin (WGA) was purchased from Sigma-Aldrich (article-no.: L9640) as lyophilized powder and used without further purification. The doubly spin-labelled tetravalent ligand (1) was synthesised in the lab of Valentin Wittmann.

25    Details of synthesis and characterisation will be published elsewhere. For the WGA-ligand samples investigated in this study solutions of WGA and the tetravalent ligand were prepared separately in deionised water. The protein concentration of the WGA solution was determined spectrophotometrically.

WGA-ligand samples were prepared by mixing WGA and ligand solutions resulting in a 2:1 molar excess of WGA compared to the ligand referring to the final sample volume. The 2-fold excess on protein was chosen to prevent free, unbound ligand in

30    solution. The sample solution was lyophilised and the resulting powder was dissolved in $D_2O$ (Magnisolv, Cas-no.: 7789200, article: S571556621) and 20 % (v/v) deuterated glycerin (Sigma-Aldrich, lot-no. MBBB5255, article: 447498-1G) as cryoprotectant. Unless stated otherwise we used a sample concentration of 160 µM WGA and 80 µM ligand. 60 µL of solution were filled into 3 mm outer diameter quartz sample tubes (ER 221 TUB/2, Part No. E221003), shock-frozen in liquid nitrogen before measurement and placed in the probe head precooled to 50 K. Samples were stored at -80 °C with unfreezing avoided.

35

## 2.2 EPR experiments

All experiments have been performed on a Bruker Elexsys E580 spectrometer at Q-band (34 GHz). The spectrometer is equipped with a SpinJet-AWG unit (Bruker) and a 150 W pulsed travelling-wave tube (TWT). All samples were measured in 3 mm outer diameter sample tubes in an overcoupled ER5106QT-2 resonator (Bruker). The quality factor Q of the overcoupled
5   resonator is approximately 200.

The samples were cooled to 50 K with a Flexline helium recirculation system (CE-FLEX-4K-0110, Bruker Biospin, ColdEdge Technologies) comprising a cold head (expander, SRDK-408D2) and a F-70H compressor (both SHI cryogenics, Tokyo, Japan), controlled by an Oxford Instruments Mercury ITC.

DEER measurements were recorded with the standard four pulse DEER sequence (Pannier et al., 2000), an 8-step phase cycle
10  (Tait and Stoll, 2016) and nuclear modulation averaging (Jeschke, 2012). The dipolar evolution time was set to 8 μs and the time step to 8 ns.

We analysed the DEER traces with DeerAnalysis2019 (Jeschke et al., 2006). We performed a background correction resulting in a background function with a dimension of $d = 3.5$. The form factor was analysed with Tikhonov regularization and a regularization parameter chosen by the generalised cross-validation criterion (Edwards and Stoll, 2018).

15  A crucial parameter for pulsed dipolar spectroscopy is the modulation-to-noise parameter $\text{MNR} = \frac{\lambda}{n}$, with the modulation depth $\lambda$ and the noise level $n$. We calculated the noise similarly to published procedures by the standard error from a fit with a smoothing spline (Bahrenberg et al., 2017; Breitgoff et al., 2019; Mentink-Vigier et al., 2013). We excluded the first 10 datapoints from the form factor because the spline typically showed some deviations at the start of the trace. Unless stated otherwise the upper limit for the noise calculation was 7 μs.

20  We used the $\eta_{2P}$-parameter which has been suggested by (Doll et al., 2015) and already been used by other authors (Doll et al., 2015; Spindler Philipp E. et al., 2013; Tait and Stoll, 2016). The $\eta_{2p}$ value is defined as the difference between two distinct time points in the DEER trace, and therefore does not require the measurement of full DEER traces. We recorded short DEER traces with 8 data points only and calculated $\eta_{2P}$ as the difference of the phase corrected DEER trace at the zero time $V(0)$ minus the first minimum of the DEER trace $V(t_{\min})$.

25  For a more detailed description of materials and methods see the Supporting Information.

## 3 Results and Discussion

In order to study the performance of DEER using different pulses, we used the doubly nitroxide-labelled tetravalent ligand bound to wheat germ agglutinin dimer (WGA) as a model system (Fig. 1). The ligand binds with a very high affinity to WGA and features a narrow distance distribution (FWHM = 0.2 nm) at 5.1 nm (to be published elsewhere). We performed DEER
30  experiments with different combinations of pulses. In the following, we will refer to a combination of rectangular observer and pump pulses as RR, to a combination of Gaussian observer and pump pulses as GG for, to a combination of rectangular observer and broadband shaped pump pulses as RS and to a combination of Gaussian observer and broadband shaped pump pulses as GS for. The preferred parameter for assessing the sensitivity of individual DEER measurements is the modulation-to-noise ratio (MNR) as defined previously.

35
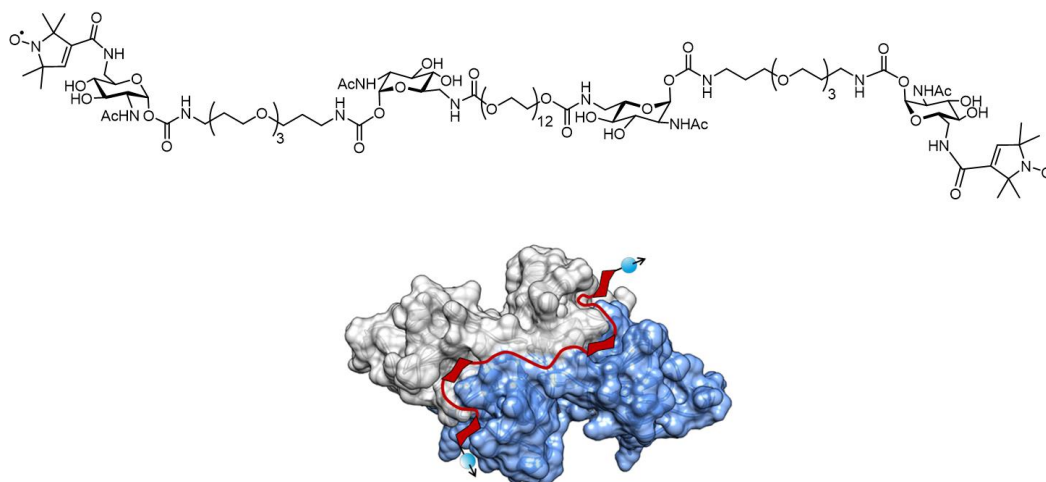
**Figure 1:** The structure of the tetravalent ligand with its two spin-(2,2,5,5-tetramethyl-3-pyrrolin-1-yloxycarbonyl)-labels and the ligand bound to WGA. The visualisation of the dimeric WGA with the subunits coloured in grey and blue is based on the crystal structure (PDB entry 2X52 (Schwefel et al., 2010)). In red, a schematic representation of the ligand is overlaid to the crystal structure. The ligand is suggested to bind with its four GlcNAc moieties to the primary binding sites of WGA. Blue balls and arrows indicate nitroxide spin labels.

### 3.1 Performance comparison for rectangular and Gaussian pulses

The pump pulse frequency was set to 34.00 GHz which is the maximum of the resonator profile (Fig. 2a). The magnetic field was set such that we pumped on the maximum of the nitroxide spectrum (Fig. 2b). To optimise the settings for RR and GG we tested observer pulses with a frequency offset of 90 MHz and 70 MHz between the pump and observer pulse, respectively. To check for different excitation profile widths of the observer pulse, we tested settings with an observer pulse amplitude of 100 % and 60 %. The pulse length was always adjusted to get $\pi/2$ and $\pi$ pulses. The observer pulse lengths for both tested frequency offsets were identical in all experiments owing to the similar values of the resonator profile at both observer frequencies (33.91 GHz and 33.93 GHz, Fig. 2a). For rectangular observer pulses the pulse lengths were 28 ns and 32 ns, for Gaussian observer pulses, they were 56 ns and 74 ns. For the pump pulse we kept the amplitude fixed at 100 %, which resulted in pulse lengths of 16 ns for rectangular and 34 ns for Gaussian pulses. As we used Gaussian pulses that were generated by Xepr, the FWHM of the Gaussian pulses was automatically defined by the software as $\mathrm{FWHM} = \frac{t_p}{2\sqrt{2\ln(2)}}$ and we did not optimise this parameter. An overview over all observer pulse settings can be found in Table S1 and S2.

For optimum observation of the spin echo modulation in DEER traces, it has been suggested to record the echo in transient mode and then perform a digital integration over a product of the recorded echo with a Gaussian filter (Pribitzer et al., 2017). This procedure is not ideal for commercial spectrometers as the transient recording of the echo drastically increases the spectrometer overhead time. Therefore, we performed a direct integration of the spin echo. We optimised the integration window for each parameter set for a maximum MNR by recording a series of Hahn echoes. Compared with commonly used integration lengths equal to the $\pi$-pulse length for rectangular pulses (Jeschke, 2007), we find settings where a 14 % increase in the SNR can be achieved by choosing a larger integration window. For Gaussian pulses, we find that it is typically preferable to choose integration windows that are shorter than the $\pi$-pulse length. More details can be found in SI 2.

**Table 1:** The rectangular and Gaussian pulses with the best performance.

| Pulse Type | Offset [MHz] | Obs. Amp. [%] | MNR | Mod depth $\lambda$ |
|---|---|---|---|---|
| **RR** | 70 | 60 | 35 | 0.31 |
| **GG** | 70 | 100 | 41 | 0.31 |

The best MNR for the setting RR was found to be 35 (Table 1). It was achieved for an offset of 70 MHz and 60 % intensity. The best MNR for GG was 41 at an offset of 70 MHz as well and a pulse amplitude of 100 % (Table 1). This corresponds to

5  a 17 % increase in the MNR of Gaussian pulses compared to rectangular pulses. This is in contrast to the findings of (Teucher and Bordignon, 2018), who found that Gaussian observer pulses have a slightly lower MNR that rectangular pulses. The exact reason for the deviating results is not entirely clear to us, we assume that this is due to their different setup with a home-built-resonator that that has slightly different properties as our commercial one.

As expected, the missing sidebands of the Gaussian pulses allow the usage of higher pulse amplitudes. This hints that for the

10  chosen parameters the pulse overlap is indeed a limiting factor for rectangular pulses. The modulation depth for RR and GG is approximately 30 % in both cases, but Gaussian pulses seem to have the advantage of a higher echo intensity, probably due to a lower pulse overlap. For RR and GG, the small offset of 70 MHz performed better than a larger offset of 90 MHz most likely due to the different echo intensities at the corresponding positions in the EPR spectrum (Fig. 2b). The results for all RR and GG setting can be found in the tables S3 and S4.
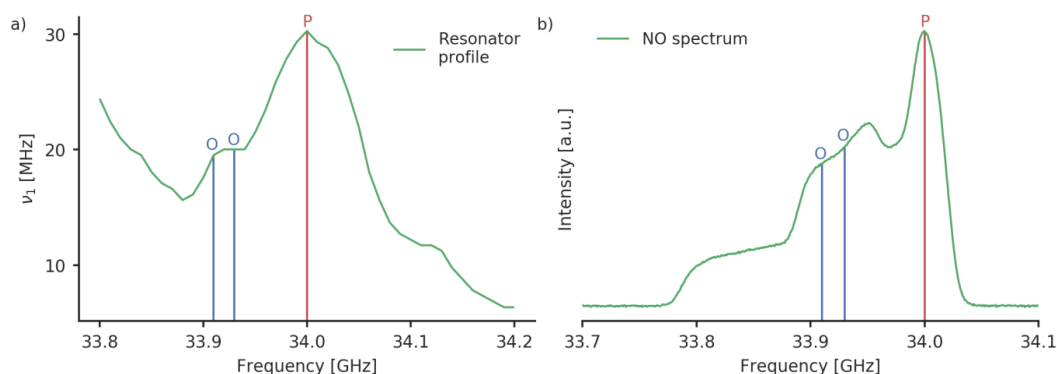
**Figure 2:** (a) Resonator profile with both tested observer frequencies (blue) and the pump (red) frequencies for the rectangular pulses and (b) the nitroxide spectrum with the positions of the two tested observer frequencies and the pump frequency.

**3.2 Broadband shaped pulses**

We set out to investigate several broadband shaped pulses, i.e. chirp, WURST, HS{1,1} and HS{1,6} pulses for the settings

20  RS and GS. Unless specified otherwise we used pump pulse lengths of 100 ns. According to Eq. (6), the pulse length of 100 ns corresponds to a minimum accessible distance of $r_{\min} = 2.75$ nm. For the determination of shorter distances we also tested chirp pulses with a length of 36 ns (referred to as short chirp pulses below), which corresponds to a distance of $r_{\min} = 1.96$ nm. Such a distance limit should be suitable for most practical applications. Furthermore, the spins are not flipped within the whole pulse duration but only a smaller fraction of it (Spindler Philipp E. et al., 2013). Simulations with an HS{1,1} pulse with a

25  length of $t_p = 100$ ns, a frequency sweep width of $\Delta f = 110$ MHz and $\beta = 8/t_p$ show distances up to $r_{\min} = 2.32$ nm could

be detectable (SI 6). It is, however, hard to generalise this effect as the spin trajectories for different broadband pulses are not necessarily the same.
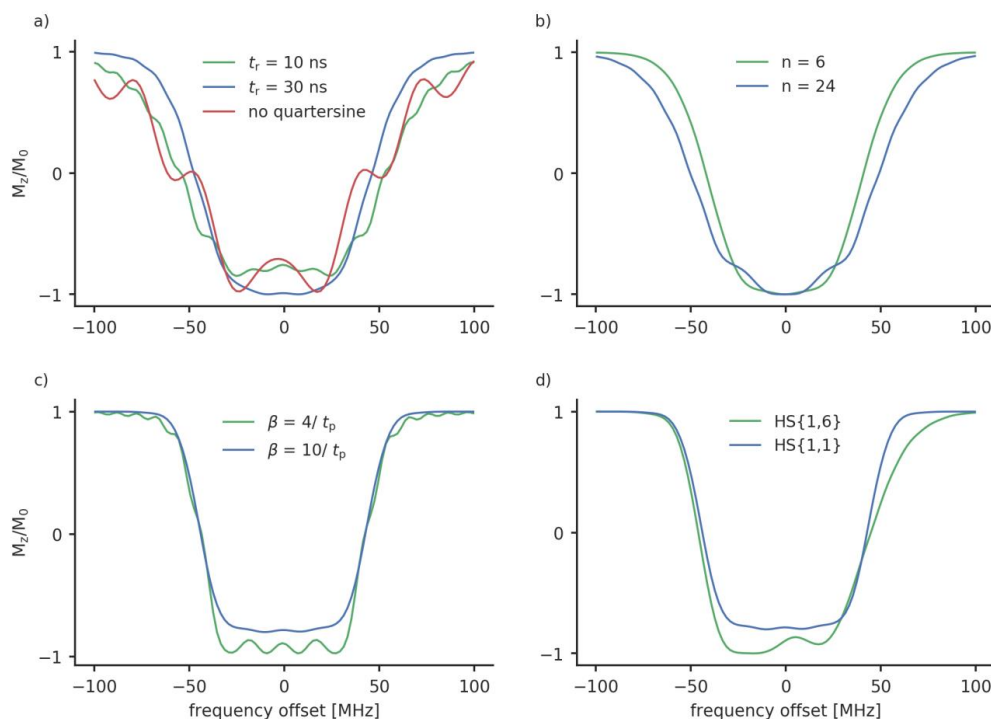
**Figure 3:** Calculated inversion profiles of broadband pulses normalised to $v_1 = 30$ MHz, which corresponds to the maximum of the measured resonator profile. a) Chirp pulses with a frequency width of 120 MHz, a length of 100 ns and a rising time of 10 ns (green), a rising time of 30 ns (blue), a length of 36 ns and no quarter-sine smoothing (red). b) WURST pulses with a frequency width of 120 MHz, a pulse length of 100 ns and a value for n of 6 (green) and 24 (blue). c) HS{1,1} pulses with a frequency width of 90 MHz and a truncation parameter of 4 (green) and 10 (blue). d) An HS{1,6} (green) and HS{1,1} (blue) pulse with a width of 90 MHz and a pulse length of 100 ns. The truncation parameter was 10 in both cases.

Figure 3 shows the calculated excitation profiles of some of the tested pulses. The calculated excitation profiles are normalised to a $v_1$ field strength of 30 MHz, which we achieved with our setup at the maximum of the resonator profile. Under such conditions, the long chirp pulses have an adiabaticity of around 5, i.e. A chirp pulse with a length of 100 ns, a sweep width of 120 MHz and a $v_1$ strength of 30 MHz has a calculated adiabaticity of 4.7. A short chirp pulse with a length of 36 ns (and otherwise unchanged parameters) has an adiabaticity of 1.7 due to the higher frequency sweep rate. Although this value is rather low, the calculations show that short chirp pulses achieve a nearly complete inversion efficiency around the maximum of the excitation profile (Fig. 3a). On the other hand, the excitation profile is rather broad with many sidebands. The finite length of the pulses creates an additional distortion. By smoothing the edge with a quarter sine, this disturbance can be reduced (Fig. 3a). A higher rising time will lead to a more properly defined excitation profile with fewer sidebands but the overall width of the excitation profile is reduced (see Fig. 3a).

WURST pulses (Fig. 3b) are characterised by an additional parameter $n$. A high value of $n$ results in a more rectangular shape of the pulse and leads to distortions in the excitation profile around the maximum (Kupce and Freeman, 1995b, 1995a; O'Dell,

2013). Small values of $n$ lead to excitation profiles with very steep and well defined side flanks. However, for small $n$ very long pulse durations are needed to achieve a high inversion efficiency. As long pulses are not feasible, because they limit the minimum distances that can be resolved, we chose to stick to 100 ns pulses and test the values for $n$ of 6, 12 and 24, for which a reasonable excitation profile can be expected (Fig. 3b).

5   In Fig. 3c we show the comparison of the excitation profile of HS{1,1} pulses for a truncation parameter of $\beta = 4/t_p$ and $\beta = 10/t_p$. For $\beta = 10/t_p$ the inversion efficiency is smaller than for $\beta = 4/t_p$, however, the excitation profile is well defined and does not show the sideband oscillations that can be seen for the latter.

Owing to their higher adiabaticity, HS{1,6} pulses feature higher inversion efficiency than HS{1,1} pulses with otherwise equal parameters (Fig. 3d), while maintaining the steep frequency flank towards the observer profile at the lower frequency
10   end.
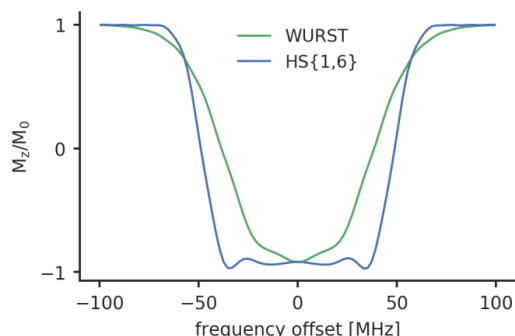
**Figure 4:** Calculated inversion profiles of a WURST ($n$ = 12, green) and a HS{1,6} (truncation parameter of $6/t_p$, blue) pulse with a pulse length of 100 ns and a sweep width of 100 MHz normalised to $\nu_1$ = 30 MHz, which corresponds to the maximum of the measured resonator profile.

15   For HS{1,1} and HS{1,6} pulses a frequency sweep width of 50 MHz to 110 MHz were tested. WURST and chirp pulses tend to have a narrower excitation profiles for a given frequency sweep width at the tested parameters (see Fig 4). We therefore chose to use higher frequency sweep widths for WURST than for HS pulses to achieve a similar excitation bandwidth.

As the bandwidth of the resonator and the width of the spectrum is limited, there is an optimum offset between the two pulses that minimises the overlap but is not too large for the resonator bandwidth. We tested offsets from a range of 70 MHz to
20   130 MHz. The offset is defined as the difference between the observer frequency and the centre of the frequency sweep of the broadband shaped pulses. For the optimisation measurements, the frequency of the observer channel was fixed and the frequency of the pump pulse was changed stepwise. We shifted the magnetic field with the pump pulse so that we always pumped on the maximum of the spectrum (see SI 1). During the increase of the offset, the position of the observer pulses in the spectrum will change as the spectrum is shifted with the pump pulse resulting in a decrease of the echo for higher offsets.
25   Table 2 shows an overview over all tested pump pulse parameter sets.

**Table 2:** The parameters for the broadband shaped pump pulses.

| Pulse type | Length [ns] | Frequency width [MHz] | Offset [MHz] | additional parameter |
|---|---|---|---|---|
| **chirp** | 100 | 80, 120, 160 200 | 70-130 | $t_r = \frac{t_p}{4}, 10$ ns, $30$ ns |
| **short chirp** | 36 | 80, 120,160, 200 | 70-130 | $t_r = \frac{t_p}{4}, 10$ ns, $30$ ns and without quarter sine smoothing |
| **WURST** | 100 | 80, 120, 160, 200 | 70-130 | $n = 6, 12, 24$ |
| **HS{1,1}** | 100 | 50, 70, 90, 110 | 70-130 | $\beta = 4/t_p, 6/t_p, 8/t_p, 10/t_p$ |
| **HS{1,6}** | 100 | 50, 70, 90, 110 | 70-130 | $\beta = 4/t_p, 6/t_p, 8/t_p, 10/t_p$ |

We used the same parameters for the observer pulses as before, meaning that we tried rectangular and Gaussian observer pulses at a microwave frequency of 33.91 GHz and 33.93 GHz at 100 % and 60 % amplitude, respectively, (see Tables S1 and S2)

5 and combined them with all the broadband shaped pulses from Table 2. This results in 504 different settings (Table 2) for the pump pulse and 8 different settings for the observer pulses, which gives a total of 4032 different DEER settings. As the measurement of full DEER traces and subsequent determination of the MNR would be very time consuming we used the $\eta_{2P}$ parameter as an estimation for the MNR. This was suggested by (Doll et al., 2015) and already used by other authors (Spindler Philipp E. et al., 2013; Tait and Stoll, 2016). As it requires only two points of the DEER trace, the measurement time can be drastically reduced. However, it has the disadvantage that artefacts, e.g. echo crossing artefacts or nuclear modulation

10 might remain undetected. Therefore, we decided to additionally perform phase cycling and nuclear modulation averaging. For different observer pulse settings, the $\eta_{2P}$ parameters are not necessarily comparable, because $\eta_{2P}$ assumes a constant absolute noise level. However, this noise level could change with different integration windows. Hence, we identified the best chirp, WURST, HS{1,1} and HS{1,6} pulse for each observer pulse setting and recorded full DEER traces of them, giving a total

15 number of 16 traces of the type RS and GS each.

Exemplary heat maps showing the $\eta_{2p}$ for Gaussian observer pulses and 100 ns pump pulses can be found in Fig. 5. We could identify several trends that were true for all observer pulse settings. HS{1,1} and HS{1,6} pulses have higher maximum $\eta_{2p}$ values than chirp and WURST pulses. HS{1,1} and HS{1,6} have their highest $\eta_{2p}$ values for smaller offsets than chirp and WURST pulses. This fits to the steeper flanks in their excitation profiles and a resulting smaller overlap with the observer

20 frequency. Nonetheless, the overall range of reasonable offsets for all pulses is rather small and within a range of 80 MHz and 100 MHz, meaning that for nitroxide-nitroxide DEER and our setup the width of the spectrum and the resonator profile has a more crucial influence in choosing the right offset than the excitation profiles of the different pump pulses. HS{1,1} and HS{1,6} pulses have smaller ideal frequency widths of 90 MHz and 110 MHz, whereas for chirp and WURST pulses the frequency widths seem to be ideal at 120 MHz and 160 MHz. This fits to the already mentioned observation, that WURST

25 pulses have smaller excitation profiles for a given sweep width with the used parameters than HS{1,1} and HS{1,6} pulses (see Fig. 4). Interestingly, despite their lower adiabaticity the short chirp pulses with a length of 36 ns had a larger $\eta_{2p}$ value than the chirps with a length of 100 ns for all observer pulse settings. Generally, we noticed that longer pump pulses lead to a reduction in the echo intensity (see also SI 13). Quarter sine smoothing does not necessarily lead to a better performance of the short chirp pulses. For the WURST pulses, a value of $n = 6$ gives the best performance with all observer pulses. For

30 different observer pulses, we find that the best performance of HS{1,1} and HS{1,6} pulses can be achieved with $\beta$ parameters ranging from $6/t_p$ to $10/t_p$.
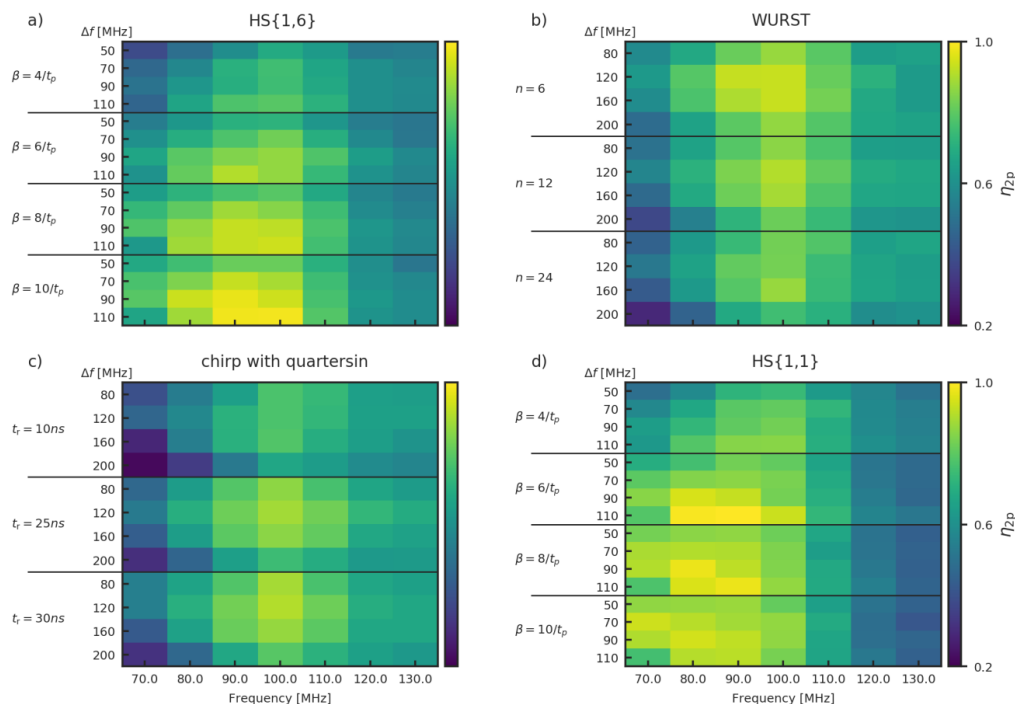
**Figure 5:** Heat maps with the $\eta_{2p}$- values for 4p-DEER measurements with an observer pulse length of 56 ns, Gaussian pulses and an integration window of 56 ns. The observer frequency is at 33.93 GHz. The pump pulse length is 100 ns. Each heat map shows a different pump pulse type: (a) HS{1,6}, (b)WURST , (c) chirp with quarter sine, and (d) HS{1,1}.

For all observer pulse settings, we identified the best parameter set for each pulse family resulting in a maximised $\eta_{2p}$. We then recorded a full DEER trace for each family and compared them by their MNRs. All results for the full DEER traces can be found in Tables S5 and S6. Table 2 shows the parameters and observer pulses that resulted in the best performing chirp, WURST, HS{1,1} and HS{1,6} pulses for the full DEER traces. We found that also for broadband shaped pump pulses

10   Gaussian observer pulses outperform rectangular ones. Again, this hints that Gaussian observer pulses can successfully reduce the frequency overlap with the pump pulse due to their missing sidebands. In all scenarios we found that an observer pulse that is positioned with a 70 MHz offset to the maximum of the resonator profile performs better than an observer pulse position with a 90 MHz offset to the maximum of the resonator profile. The offset to the broadband shaped pump pulse, however, does not change on average, which means that in the former case the observer and pump pulse have a more symmetric positioning

15   around the maximum.

**Table 3:** The parameters of the observer and pump pulse that gave the best MNR for each pump pulse type. All observer pulses are Gaussian pulses with a pulse length of 74 ns for a 60 % intensity and 56 ns for a 100 % intensity. The observer frequency was 33.93 GHz in all cases. The MNR was evaluated up to 7 µs.

| Pump pulse | Obs. Amp. [%] | $t_\pi$ [ns] | $\Delta f$ [MHz] | Offset [MHz] | MNR | Mod depth $\lambda$ |
|---|---|---|---|---|---|---|
| **HS{1,6}** ($\beta = 10/t_p$) | 60 | 100 | 110 | 90 | 45 | 0.61 |
| **WURST** ($n$=6) | 60 | 100 | 160 | 90 | 40 | 0.63 |
| **Chirp** (no smoothing) | 100 | 36 | 120 | 80 | 45 | 0.49 |
| **HS{1,1}** ($\beta = 8/t_p$) | 100 | 100 | 110 | 90 | 50 | 0.52 |

5   Broadband shaped pump pulses lead to a larger modulation depth as rectangular and Gaussian pulses. Whereas for non-broadband pulses the modulation depth is limited to around 30 % with our setup, we achieved an increase of up to 63 % with WURST pulses. HS{1,6} pulses also lead to high modulation depths of 61 %. For chirp and HS{1,1} pulses smaller modulation depths of approx. 50 % were observed. However, the highest modulation depth will not necessarily lead to the highest MNR as can be seen in Table 3. This is due to a larger background decay of pulses with a higher inversion efficiency and will be

10   analysed in the next section. Due to a higher bandwidth overlap, broadband shaped pulses will also reduce the echo intensity stronger than rectangular or Gaussian pulses. HS{1,1} pulses seem to be a good compromise between a high modulation depth, a high echo intensity and a background decay that is not too steep. They resulted in the highest MNR of 50 with a pulse length of 100 ns, an offset of 90 MHz, a frequency bandwidth of 110 MHz and $\beta = 8/t_p$ with the observer pulses being Gaussian pulses with an amplitude of 100 % and a frequency of 33.93 GHz. Interestingly, this performance is achieved although the

15   broadband pulse does not achieve a complete inversion (Fig. S6d). The modulation depth in that case increased to 52 % (Fig. S8). This corresponds to an MNR increase of 43 % compared to RR and 22 % compared to GG. To estimate the lower limit of distances that can be determined with such a 100 ns pulse, we performed a simulation to see when the spins are actually flipped during the experiment (see S12). Most spins are flipped between 20 ns and 80 ns within the pulse duration, making it an effective length of 60 ns where the spins flips occurs, which would correspond to a minimum detectable distance limit of

20   2.3 nm instead of 2.8 nm for a 100 ns spin flip period.

The comparison of pulses with and without bandwidth compensation as suggested by (Doll et al., 2013) showed that a bandwidth compensation does not give a significant advantage in the $\eta_{2p}$ value under our conditions (S11). This is probably due to the rather flat resonator profile in the region with maximum sensitivity where the pump pulse is applied.

We have also compared broadband pulses with a length of 100 ns and 200 ns (see SI 12). The 200 ns pulses seem to perform

25   worse for most pulse types than the 100 ns pulses. Particularly, we observed that a longer pump pulse can reduce the echo intensity (see SI 13). As the reason is not absolutely clear to us for now, we decided to stick to 100 ns pulses.

30

### 3.3 Background behaviour

As stated by equation (10) the measured raw data does not only consist of the desired form factor but includes a background contribution emerging from intermolecular interactions. A common way to deal with this, is to fit the background according to equation (11) and divide the raw data by the fit to obtain the form factor that can then be transformed into a distance

5 distribution (Jeschke, 2012; Jeschke et al., 2006). This method, however, leads to an increase in the noise level towards the end of the trace which can significantly disturb the reliability of the distance distribution, as recently shown by (Fábregas Ibáñez and Jeschke, 2020). They suggested alternative methods to correct for the background. We will, however, limit this discussion to a background correction method by division as it is very common.

The broader excitation profile of broadband shaped pulses will also increase the background decay which results in a higher

10 noise level of broadband shaped pump pulses compared to rectangular or Gaussian pump pulses. We find an approximately linear relation between the modulation depth and the background decay (SI 17). To investigate this effect more deeply we evaluated the MNR of the experimental DEER form factors excluding the later part of the form factor and only taking into account the first part up to a truncation time $\tau_{\mathrm{truncation}}$. Truncation the DEER trace will not change the modulation depth, but due to the background decay, the noise level will be different. Figure 6 shows the MNR of broadband pulses as a function of

15 the truncation time $\tau_{\mathrm{truncation}}$. As expected, the MNR decreases with increasing $\tau_{\mathrm{truncation}}$ for all pulses, because of the increase of the noise. However, the rate of the decrease in MNR is different for different pulse types, which means that the relative performance of the pulses also depends on the length of the DEER trace and therefore on the distance between the spin centres that is supposed to be measured.
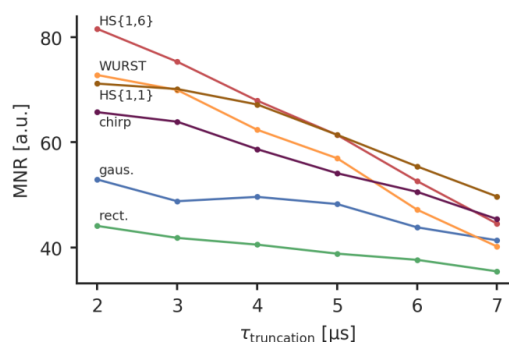
20 **Figure 6:** The MNR value as a function of the dipolar evolution time up to which the noise has been evaluated, i.e. the truncation time $\tau_{\mathrm{truncation}}$. The sample has a concentration of 80 µM of spin-labelled ligand. The line between the points is only a guidance for the eyes.

It turns out that HS{1,6} and WURST pulses with their higher modulation depths have the highest MNR for short DEER traces, whereas for longer traces HS{1,1} and chirp pulses are better. The background decay seems to play a decisive role for

25 the MNR and the pulses resulting in a high modulation depth also have a larger background decay. As the background decay causes the noise level to increase with increasing dipolar evolution time, its influence is less pronounced for short DEER traces, where the high modulation depth seems to be leading to a high MNR. For longer traces, a high modulation depth is linked to a strong background decay and a high noise level towards the end of the trace. Therefore, the MNR of pump pulses generating a high modulation depth decreases stronger than for pulses effecting a smaller modulation depth. This means that HS{1,1} and

30 chirp pulses perform better for longer traces.

As rectangular and Gaussian pump pulses have rather small modulation depths, the corresponding decrease of the MNR due to the background decay is also rather small, that means that the improvement achievable with broadband shaped pulses is greater for shorter DEER traces. For short truncation times $\tau_{\text{truncation}}$ of 2 µs we observe an increase in MNR from 44 for rectangular pulses (RR) to 82 for the best broadband shaped pulse (RS), which was an HS{1,6} pulse in this case. This corresponds to an increase of 86 %. For long truncation times $\tau_{\text{truncation}}$ of 7 µs, this increase goes down to 43 %. This means that the MNR improvement that can be achieved by broadband shaped pulses can be drastically dependent on the length of the measured DEER trace and therefore on the distance range to be covered by the measurement. The performance of all the pulses at $\tau_{\text{truncation}} = 2$ µs can be found in Tables S7-S10. The chirp, WURST, HS{1,1} and HS{1,6} pulse resulting in the best MNR are summarized in Table 4. For the broadband shaped pulses there were some minor changes in the parameters that gave the MNR when the truncation time was set to a shorter value of $t_{\text{truncation}} = 2$ µs. For RR and GG there were changes in the best parameter settings.

**Table 4:** The parameters of the observer and pump pulse resulting in the best MNR for each pulse type when the MNR was evaluated up to $\tau_{\text{truncation}} = 2\mu s$. All observer pulses are Gaussian pulses with a pulse length of 74 ns for 60 % intensity and 56 ns for 100 % intensity. The observer frequency was 33.93 GHz for all pulses.

| Pump pulse | Obs. Amp. [%] | $t_\pi$ [ns] | $\Delta f$ [MHz] | Offset [MHz] | MNR | Mod depth $\lambda$ |
|---|---|---|---|---|---|---|
| **HS{1,6}** ($\boldsymbol{\beta = 10/t_p}$) | 60 | 100 | 110 | 90 | 82 | 0.61 |
| **WURST** (**n**=6) | 100 | 100 | 160 | 90 | 73 | 0.63 |
| **Chirp** (no smoothing) | 100 | 36 | 120 | 80 | 65 | 0.49 |
| **HS{1,1}** ($\boldsymbol{\beta = 8/t_p}$) | 60 | 100 | 110 | 80 | 74 | 0.52 |

The background correction by division is particularly susceptible for a steep background decay and other methods give more reliable distance distributions even if the background decay is high (Fábregas Ibáñez and Jeschke, 2020). Hence, the MNR values determined here cannot be directly converted in the reliability of the determined distance distribution, because this does additionally depend on the method that is used for background correction. However, all proposed methods suffer from less reliable distance distributions when the background decay gets higher, so the underlying problem is always present.

### 3.4 Concentration dependence

To check for a concentration dependent performance of broadband shaped pulses we also prepared a sample with a lower concentration of 30 µM ligand and 60 µM WGA and performed DEER measurements with the optimised parameter settings for the short chirp, WURST, HS{1,1} and HS{1,6} pulses. We did, however, not check observer frequencies of 33.91 GHz, since they always performed worse than an observer position of 33.93 GHz. For RR we tested an offset of 70 MHz and 60 % intensity, for GG we tested an offset of 70 MHz as well, but an intensity of 100 %, as these settings performed best before.

This sample showed almost no background for all pulses (see SI 18). As the influence of the background is minimised due to the low concentration we expected to find the trends as for the case of the high concentrated samples and short truncation times. Figure 7 shows the MNR as function of the truncation time point $\tau_{\text{truncation}}$ up to which the noise has been evaluated. As expected, no significant decrease of the MNR with higher truncation times $\tau_{\text{truncation}}$ was found. Without a significant background the noise towards the end of the background-corrected form factor does not increase significantly. The decrease

of the MNR found for the high concentration sample was therefore not observed here. For some pulses there is a slight increase in the MNR, however, we assigned this behaviour to a numerical uncertainty in the analysis.
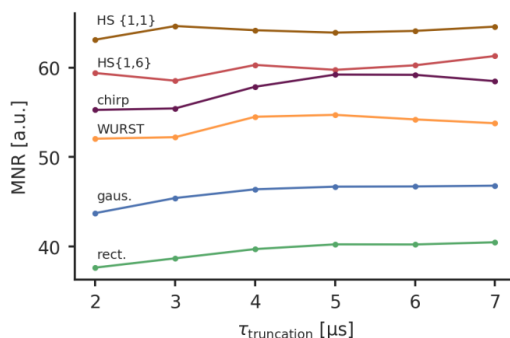
**Figure 7:** The MNR as a function of the dipolar evolution time up to which the noise has been evaluated. The sample has a
5  concentration of 30 µM of spin-labelled ligand.

**Table 5:** The parameters of the observer and pump pulse resulting in the best MNR for each pulse type. All observer pulses are Gaussian pulses with pulse lengths of 74 ns for 60 % intensity and 56 ns for 100 % intensity. The observer frequency was 33.93 GHz for all pulses. The MNR was evaluated up to 7 µs.

| Pump pulse | Obs. Amp. [%] | $t_\pi$ [ns] | $\Delta f$ [MHz] | Offset [MHz] | MNR | Mod depth $\lambda$ |
|---|---|---|---|---|---|---|
| **HS{1,6} ($\beta = 10/t_p$)** | 100 | 100 | 110 | 90 | 61 | 0.55 |
| **WURST ($n$=6)** | 60 | 100 | 160 | 100 | 54 | 0.59 |
| **Chirp** (no smoothing) | 100 | 36 | 120 | 80 | 58 | 0.46 |
| **HS{1,1} ($\beta = 8/t_p$)** | 100 | 100 | 110 | 90 | 65 | 0.47 |

10  With the low concentration sample, we found an MNR of 40 and a modulation depth of 31 % for rectangular pulses, for Gaussian pulses we found an MNR of 47 and a modulation depth of 30 %. Thus, also at lower spin concentrations the Gaussian pulses lead to a similar modulation depth as rectangular pulses, but again to an overall higher MNR. Table 5 shows the results for the different broadband shaped pump pulses in combination with the observer pulse with whom they performed best.

Table 5 shows the optimised parameters for the different pump pulses. All results can be found in Table S11. The parameters
15  found for the observer and pump pulses differ slightly from the parameters identified for the high concentration sample, but lie in a similar range.

The broadband shaped pump pulses resulted in a modulation depth that is a bit lower than for the sample with the high concentration. The MNR was lower as well. Furthermore, the order of performance of the different pulse types changed. While we expected HS{1,6} and WURST pulses with their high modulation depths to perform better than HS{1,1} and chirp pulses
20  for a sample less susceptible to background influence, HS{1,1} pulses were actually performing best and WURST pulses were the worst broadband shaped pulses. HS{1,1} pulses lead to an increase in the MNR of 60 % compared to rectangular pulses. This is also lower than the 86 % increase that was obtained for the 80 µM ligand concentration. The reason for the change of this behaviour is probably a difference in the resonator profile that we noticed compared to the other sample with the higher

concentration (see SI 20). The achieved $B_1$ field was a bit lower for this sample which changes the performance of the pulses. However, HS{1,1} and HS{1,6} pulses both give a good MNR with a high concentration as well as with a low concentration.

We also performed analytical calculations to get a more quantitative estimate for the MNR increase of broadband shaped pulses depending on the trace length and the spin concentration (see SI 19). They show that the latter two have a significant
5    effect on the performance improvement that can be expected when using a broadband shaped pulse. However, for concentrations typically used in DEER experiments, a sensitivity increase can always be expected when using broadband shaped pulses instead of monochromatic pulses.

## 4 Conclusion and Outlook

We have compared various broadband shaped pulses as pump pulses for DEER spectroscopy in Q-band performed on samples
10   with nitroxide spin labels and investigated under which circumstances they perform best. By increasing the inversion profile, broadband shaped pulses can increase the modulation depth from 30 % with rectangular pulses up to 60 %. However, with a larger inversion profile of broadband shaped pulses the overlap with the observer pulse and the background decay will also increase. Both of those effects will tend to reduce the MNR. The overall MNR increase will therefore be a compromise between the increase in the modulation depth and the smaller echo and larger background
15   contribution.

Systematic analysis of a trial-and-error optimisation has yielded that the performance of broadband shaped pulses depends on the dipolar evolution time and the concentration of spin centres. Larger dipolar evolution times mean that the background has decayed stronger by the end of the form factor. Pulses with a higher inversion efficiency will produce a larger background decay and their performance decreases stronger for longer traces than for pulses with a smaller inversion efficiency. We found
20   HS{1,1} and HS{1,6} in combination with Gaussian observer pulses to give a good MNR for high as well as low spin concentrations. HS{1,1} have a lower inversion efficiency and therefore a lower modulation depth but they perform better with longer traces. The exact parameters depend on the setup, but with values of $\beta = 8/t_p$ or $\beta = 10/t_p$, $t_p = 100$ ns, $\Delta f = 110$ MHz and an offset of 80 MHz or 90 MHz we typically achieved good results. If a high modulation depth should be achieved, WURST pulses are the best pulses. Good parameters are $n = 6$, $t_p = 100$ ns, $\Delta f = 160$ MHz and an offset of 90 MHz
25   or 100 MHz.

## 5 Data availability

The raw data can be downloaded at https://doi.org/10.5281/zenodo.3660242 (Scherer et al., 2020).

## 6 Author contribution

30   AS, ST, SW and MD conceived the research idea and designed the conducted experiments. AS conducted the EPR experiments and analysed the results with ST. The spin labelled ligand was synthesised in the lab of VW. AS prepared all the figures and wrote the draft manuscript. All authors discussed the results and revised the manuscript.

## 7 Competing interests

The authors declare no conflict of interests.

35

## 8 Acknowledgements

We thank Philipp Rohse for the synthesis of the spin labelled ligand. Jörg Fischer is thanked for sample preparation. This project has received funding from the European Research Council (ERC) under the European Union's Horizon 2020 research and innovation programme (Grant Agreement number: 772027 — SPICE — ERC-2017-COG). A.S. gratefully acknowledges

5   financial support from the Zukunftskolleg of the University of Konstanz. A.S., S.T. and S.W. gratefully acknowledge financial support from the Konstanz Research School Chemical Biology (KoRS-CB).

## 9 References

Abdullin, D., Duthie, F., Meyer, A., Müller, E. S., Hagelueken, G. and Schiemann, O.: Comparison of PELDOR and RIDME for Distance Measurements between Nitroxides and Low-Spin Fe(III) Ions, J. Phys. Chem. B, 119(43), 13534–13542,

10   doi:10.1021/acs.jpcb.5b02118, 2015.

Bahrenberg, T., Rosenski, Y., Carmieli, R., Zibzener, K., Qi, M., Frydman, V., Godt, A., Goldfarb, D. and Feintuch, A.: Improved sensitivity for W-band Gd(III)-Gd(III) and nitroxide-nitroxide DEER measurements with shaped pulses, J. Magn. Reson., 283(Supplement C), 1–13, doi:10.1016/j.jmr.2017.08.003, 2017.

Baum, J., Tycko, R. and Pines, A.: Broadband and adiabatic inversion of a two-level system by phase-modulated pulses,

15   Phys. Rev. A, 32(6), 3435, 1985.

Bohlen, J. M. and Bodenhausen, G.: Experimental Aspects of Chirp NMR Spectroscopy, J. Magn. Reson. A, 102(3), 293–301, doi:10.1006/jmra.1993.1107, 1993.

Borbat, P. P., Georgieva, E. R. and Freed, J. H.: Improved Sensitivity for Long-Distance Measurements in Biomolecules: Five-Pulse Double Electron–Electron Resonance, J. Phys. Chem. Lett., 4(1), 170–175, doi:10.1021/jz301788n, 2013.

20   Breitgoff, F. D., Soetbeer, J., Doll, A., Jeschke, G. and Polyhach, Y. O.: Artefact suppression in 5-pulse double electron electron resonance for distance distribution measurements, Phys. Chem. Chem. Phys., 19(24), 15766–15779, 2017.

Breitgoff, F. D., Keller, K., Qi, M., Klose, D., Yulikov, M., Godt, A. and Jeschke, G.: UWB DEER and RIDME distance measurements in Cu(II)–Cu(II) spin pairs, J. Magn. Reson., doi:10.1016/j.jmr.2019.07.047, 2019.

Collauto, A., Feintuch, A., Qi, M., Godt, A., Meade, T. and Goldfarb, D.: Gd(III) complexes as paramagnetic tags: Evaluation

25   of the spin delocalization over the nuclei of the ligand, J. Magn. Reson., 263(Supplement C), 156–163, doi:10.1016/j.jmr.2015.12.025, 2016.

Dalaloyan, A., Qi, M., Ruthstein, S., Vega, S., Godt, A., Feintuch, A. and Goldfarb, D.: Gd(iii)-Gd(iii) EPR distance measurements - the range of accessible distances and the impact of zero field splitting, Phys. Chem. Chem. Phys., 17(28), 18464–18476, doi:10.1039/C5CP02602D, 2015.

30   Deschamps, M., Kervern, G., Massiot, D., Pintacuda, G., Emsley, L. and Grandinetti, P. J.: Superadiabaticity in magnetic resonance, J. Chem. Phys., 129(20), 204110, doi:10.1063/1.3012356, 2008.

Di Valentin, M., Albertini, M., Zurlo, E., Gobbo, M. and Carbonera, D.: Porphyrin Triplet State as a Potential Spin Label for Nanometer Distance Measurements by PELDOR Spectroscopy, J. Am. Chem. Soc., 136(18), 6582–6585, doi:10.1021/ja502615n, 2014.

35   Doll, A. and Jeschke, G.: Wideband frequency-swept excitation in pulsed EPR spectroscopy, Spec. Issue Methodol. Adv. EPR Spectrosc. Imaging, 280, 46–62, doi:10.1016/j.jmr.2017.01.004, 2017.

Doll, A., Pribitzer, S., Tschaggelar, R. and Jeschke, G.: Adiabatic and fast passage ultra-wideband inversion in pulsed EPR, J. Magn. Reson., 230, 27–39, doi:10.1016/j.jmr.2013.01.002, 2013.

Doll, A., Qi, M., Wili, N., Pribitzer, S., Godt, A. and Jeschke, G.: Gd(III)–Gd(III) distance measurements with chirp pump

40   pulses, J. Magn. Reson., 259(Supplement C), 153–162, doi:10.1016/j.jmr.2015.08.010, 2015.

Doll, A., Qi, M., Godt, A. and Jeschke, G.: CIDME: Short distances measured with long chirp pulses, J. Magn. Reson., 273, 73–82, doi:10.1016/j.jmr.2016.10.011, 2016.

Edwards, T. H. and Stoll, S.: Optimal Tikhonov regularization for DEER spectroscopy, J. Magn. Reson., 288, 58–68, doi:10.1016/j.jmr.2018.01.021, 2018.

5   Fábregas Ibáñez, L. and Jeschke, G.: Optimal background treatment in dipolar spectroscopy, Phys. Chem. Chem. Phys., 22(4), 1855–1868, doi:10.1039/C9CP06111H, 2020.

Garwood, M. and DelaBarre, L.: The Return of the Frequency Sweep: Designing Adiabatic Pulses for Contemporary NMR, J. Magn. Reson., 153(2), 155–177, doi:10.1006/jmre.2001.2340, 2001.

Grytz, C. M., Kazemi, S., Marko, A., Cekan, P., Guntert, P., Sigurdsson, S. T. and Prisner, T. F.: Determination of helix
10   orientations in a flexible DNA by multi-frequency EPR spectroscopy, Phys. Chem. Chem. Phys., 19(44), 29801–29811, doi:10.1039/C7CP04997H, 2017.

Hintze, C., Bücker, D., Domingo Köhler, S., Jeschke, G. and Drescher, M.: Laser-Induced Magnetic Dipole Spectroscopy, J. Phys. Chem. Lett., 7(12), 2204–2209, doi:10.1021/acs.jpclett.6b00765, 2016.

Hubbell, W. L., Gross, A., Langen, R. and Lietzow, M. A.: Recent advances in site-directed spin labeling of proteins, Curr.
15   Opin. Struct. Biol., 8(5), 649–656, doi:10.1016/S0959-440X(98)80158-9, 1998.

Jassoy, J. J., Meyer, A., Spicher, S., Wuebben, C. and Schiemann, O.: Synthesis of Nanometer Sized Bis-and Tris-trityl Model Compounds with Different Extent of Spin–Spin Coupling, Molecules, 23(3), 682, 2018.

Jeschke, G.: Instrumentation and experimental setup, in ESR spectroscopy in membrane biophysics, vol. 27, edited by M. A. Hemminga and L. Berliner, pp. 17–47, Springer Science & Business Media., 2007.

20   Jeschke, G.: DEER Distance Measurements on Proteins, Annu. Rev. Phys. Chem., 63(1), 419–446, doi:10.1146/annurev-physchem-032511-143716, 2012.

Jeschke, G., Bender, A., Paulsen, H., Zimmermann, H. and Godt, A.: Sensitivity enhancement in pulse EPR distance measurements, J. Magn. Reson., 169(1), 1–12, doi:10.1016/j.jmr.2004.03.024, 2004.

Jeschke, G., Chechik, V., Ionita, P., Godt, A., Zimmermann, H., Banham, J., Timmel, C. R., Hilger, D. and Jung, H.:
25   DeerAnalysis2006—a comprehensive software package for analyzing pulsed ELDOR data, Appl. Magn. Reson., 30(3), 473–498, doi:10.1007/BF03166213, 2006.

Kobzar, K., Ehni, S., Skinner, T. E., Glaser, S. J. and Luy, B.: Exploring the limits of broadband 90° and 180° universal rotation pulses, J. Magn. Reson., 225, 142–160, doi:10.1016/j.jmr.2012.09.013, 2012.

Kupce, E. and Freeman, R.: Adiabatic Pulses for Wideband Inversion and Broadband Decoupling, J. Magn. Reson. A, 115(2),
30   273–276, doi:10.1006/jmra.1995.1179, 1995a.

Kupce, Ē. and Freeman, R.: Stretched Adiabatic Pulses for Broadband Spin Inversion, J. Magn. Reson. A, 117(2), 246–256, doi:10.1006/jmra.1995.0750, 1995b.

Kupce, Ē. and Freeman, R.: Optimized Adiabatic Pulses for Wideband Spin Inversion, J. Magn. Reson. A, 118(2), 299–303, doi:10.1006/jmra.1996.0042, 1996.

35   Kuzhelev, A. A., Akhmetzyanov, D., Denysenkov, V. P., Krumkacheva, O., Shevelev, G., Bagryanskaya, E. and Prisner, T. F. F.: High-frequency pulsed electron-electron double resonance spectroscopy on DNA duplexes using trityl tags and shaped microwave pulses, Phys. Chem. Chem. Phys., doi:10.1039/C8CP03951H, 2018.

Lovett, J. E., Lovett, B. W. and Harmer, J.: DEER-Stitch: Combining three- and four-pulse DEER measurements for high sensitivity, deadtime free data, J. Magn. Reson., 223, 98–106, doi:10.1016/j.jmr.2012.08.011, 2012.

40   Mahawaththa, M., Lee, M., Giannoulis, A., Adams, L. A., Feintuch, A., Swarbrick, J., Graham, B., Nitsche, C., Goldfarb, D. and Otting, G.: Small Neutral Gd(III) Tags for Distance Measurements in Proteins by Double Electron-Electron Resonance Experiments, Phys. Chem. Chem. Phys., doi:10.1039/C8CP03532F, 2018.

Mentink-Vigier, F., Collauto, A., Feintuch, A., Kaminker, I., Tarle, V. and Goldfarb, D.: Increasing sensitivity of pulse EPR experiments using echo train detection schemes, J. Magn. Reson., 236, 117–125, doi:10.1016/j.jmr.2013.08.012, 2013.

Milikisiyants, S., Voinov, M. A., Marek, A., Jafarabadi, M., Liu, J., Han, R., Wang, S. and Smirnov, A. I.: Enhancing sensitivity of Double Electron-Electron Resonance (DEER) by using Relaxation-Optimized Acquisition Length Distribution (RELOAD) scheme, J. Magn. Reson., 298, 115–126, doi:10.1016/j.jmr.2018.12.004, 2019.

Milov, A. D., Ponomarev, A. B. and Tsvetkov, Y. D.: Electron-electron double resonance in electron spin echo: Model biradical systems and the sensitized photolysis of decalin, Chem. Phys. Lett., 110(1), 67–72, doi:10.1016/0009-2614(84)80148-7, 1984.

Milov, A.D., Salikhov, K.M. and Shirov, M.D.: Use of the double resonance in electron spin echo method for the study of paramagnetic center spatial distribution in solids., Fiz Tverd Tela, 23(1), 975–982, 1981.

O'Dell, L. A.: The WURST kind of pulses in solid-state NMR, Solid State Nucl. Magn. Reson., 55–56, 28–41, doi:10.1016/j.ssnmr.2013.10.003, 2013.

Pannier, M., Veit, S., Godt, A., Jeschke, G. and Spiess, H. .: Dead-Time Free Measurement of Dipole–Dipole Interactions between Electron Spins, J. Magn. Reson., 142(2), 331–340, doi:10.1006/jmre.1999.1944, 2000.

Polyhach, Y., Bordignon, E., Tschaggelar, R., Gandra, S., Godt, A. and Jeschke, G.: High sensitivity and versatility of the DEER experiment on nitroxide radical pairs at Q-band frequencies, Phys. Chem. Chem. Phys., 14(30), 10762–10773, doi:10.1039/C2CP41520H, 2012.

Pribitzer, S., Sajid, M., Hülsmann, M., Godt, A. and Jeschke, G.: Pulsed triple electron resonance (TRIER) for dipolar correlation spectroscopy, J. Magn. Reson., 282, 119–128, doi:10.1016/j.jmr.2017.07.012, 2017.

Robotta Marta, Gerding Hanne R., Vogel Antonia, Hauser Karin, Schildknecht Stefan, Karreman Christiaan, Leist Marcel, Subramaniam Vinod and Drescher Malte: Alpha-Synuclein Binds to the Inner Membrane of Mitochondria in an α-Helical Conformation, ChemBioChem, 15(17), 2499–2502, doi:10.1002/cbic.201402281, 2014.

Scherer, A., Tischlik, S., Weickert, S., Wittmann, V. and Drescher, M.: Raw data for "Optimising broadband pulses for DEER depends on concentration and distance range of interest," , doi:10.5281/zenodo.3660242, 2020.

Schwefel, D., Maierhofer, C., Beck, J. G., Seeberger, S., Diederichs, K., Möller, H. M., Welte, W. and Wittmann, V.: Structural Basis of Multivalent Binding to Wheat Germ Agglutinin, J. Am. Chem. Soc., 132(25), 8704–8719, doi:10.1021/ja101646k, 2010.

Spindler, P. E., Schöps, P., Kallies, W., Glaser, S. J. and Prisner, T. F.: Perspectives of shaped pulses for EPR spectroscopy, J. Magn. Reson., 280(Supplement C), 30–45, doi:10.1016/j.jmr.2017.02.023, 2017.

Spindler Philipp E., Glaser Steffen J., Skinner Thomas E. and Prisner Thomas F.: Broadband Inversion PELDOR Spectroscopy with Partially Adiabatic Shaped Pulses, Angew. Chem. Int. Ed., 52(12), 3425–3429, doi:10.1002/anie.201207777, 2013.

Tait, C. E. and Stoll, S.: Coherent pump pulses in Double Electron Electron Resonance spectroscopy, Phys. Chem. Chem. Phys., 18(27), 18470–18485, doi:10.1039/C6CP03555H, 2016.

Tannús, A. and Garwood, M.: Improved Performance of Frequency-Swept Pulses Using Offset-Independent Adiabaticity, J. Magn. Reson. A, 120(1), 133–137, doi:10.1006/jmra.1996.0110, 1996.

Teucher, M. and Bordignon, E.: Improved signal fidelity in 4-pulse DEER with Gaussian pulses, J. Magn. Reson., 296, 103–111, doi:10.1016/j.jmr.2018.09.003, 2018.

Wort, J., Ackermann, K., Giannoulis, A., Stewart, A., Norman, D. and Bode, B. E.: Sub-micromolar pulse dipolar EPR spectroscopy reveals increasing CuII-labelling of double-histidine motifs with lower temperature., Angew. Chem., 0(ja), doi:10.1002/ange.201904848, 2019.